communications materials

ARTICLE

https://doi.org/10.1038/s43246-021-00164-9 OPEN

Enhanced aging kinetics in Al-Mg-Si alloys by up-quenching

Florian Schmid [1✉], Philip Dumitraschkewitz[2], Thomas Kremmer [2], Peter J. Uggowitzer[2], Ramona Tosone[3] & Stefan Pogatscher [1,2✉]

Precipitation-hardened aluminium alloys typically obtain their strength by forming second-phase particles, which, however, often have a negative effect on formability. To enable both lightweight construction and forming of complex parts such as body panels, high strength and formability are required simultaneously. Cluster hardening is a promising approach to achieve this. Here, we show that short thermal spikes, denoted as up-quenching, increase aging kinetics, which we attribute to the repeated process of vacancies being formed at high temperatures and retained when cooled to lower temperatures. Combined with further heat treatment, the up-quenching process promotes rapid and extensive cluster formation in Al-Mg-Si alloys, which in turn generates significant strengthening at industrially relevant heat treatment time scales. The high elongation values also observed are attributed to reduced solute depleted zones along grain boundaries.

[1] Christian Doppler Laboratory for Advanced Aluminum Alloys, Chair of Nonferrous Metallurgy, Montanuniversitaet Leoben, Leoben, Austria. [2] Chair of Nonferrous Metallurgy, Montanuniversitaet Leoben, Leoben, Austria. [3] AMAG rolling GmbH, Ranshofen, Austria. ✉email: florian.schmid@unileoben.ac.at; stefan.pogatscher@unileoben.ac.at

Aluminium alloys are deployed in a wide field of applications due to their outstanding mix of properties: tuneable strength and formability, good corrosion resistance and machinability, and an advantageous strength-to-weight ratio[1]. Precipitation hardening, discovered by accident in the early 20th century[2,3], is considered to be one of aluminium alloys' most important strengthening mechanisms and has long been the focus of intensive development. However, this often involves a trade-off between strength and formability because conventional (often isothermal) heat treatment strategies generate ductility-reducing precipitate free zones[4] and coarse, unevenly distributed precipitates[5–7].

Clusters can also form in aluminium alloys during aging at low to medium temperatures. In contrast to conventional precipitates (θ/S-phase and its precursors in Al–Cu(–Mg) alloys; β-phase and its precursors in Al–Mg–Si alloys; or η-phase and its precursors in Al–Zn(–Mg) alloys), clusters are defined by Dumitraschkewitz et al.[8] as local aggregation of alloying atoms without a detectable structure or ordering, and we use that definition here. Clusters form from the super-saturated solid solution created through accelerated diffusion brought about by an excess of vacancies at low temperatures, leading to a decrease in the overall Gibbs free energy. However, they are only stable up to certain temperatures (for example, the solvus temperature of Mg,Si-co-clusters formed at room temperature is around 170 °C in the Al–Mg–Si alloy EN AW-6016[9]), which limits any further increase in reaction kinetics. The details of strengthening via clusters are not yet fully clear, but some models link the effect to order or configurational strengthening[10] and to modulus hardening[11], as demonstrated by Starink et al.[9,12] for both 2xxx and 6xxx Al alloys. It has also been reported that clusters can even show a greater increase in strength per unit volume fraction than the β″-precipitates in Al–Mg–Si alloys, which are typically formed due to artificial aging[13,14]. However, when materials are subjected to conventional aging procedures, cluster hardening, because of clusters' lower volume fraction, does not generate the high strength levels possible via precipitation formation. The important point here is that some aluminium alloys strengthened by clusters have primarily shown enhanced ductility at strength values comparable to those of classical artificial aging schemes. One explanation for this behaviour seen in literature is that repartitioning of solutes into the matrix takes place during deformation, with no negative effect on strain hardening[15,16]. Another possibility may be reduced precipitate free zones alongside grain boundaries in materials strengthened by clusters formed at low temperatures. Precipitate-free zones can reduce the ductility of precipitation-hardened materials, as strain accumulates in these soft regions and accelerates material failure[4]. The low aging temperatures necessary for the formation of clusters curtail the formation of precipitation free zones (PFZs), which can be considered a positive side effect[17]. Recently, it has also been shown that extensive cluster formation promoted by excess vacancies leads to a strengthening of otherwise weak precipitate-free zones along grain boundaries[18].

To promote extensive cluster formation for the purpose of generating strong strengthening, two processing options can be applied: (i) very long-term medium-temperature aging; and (ii) cyclic deformation after quenching.

When aged at 100 °C for 25 days, an Al–Mg–Si alloy shows a high yield strength which is comparable to that after conventional artificial aging, as shown by Takata et al.[16]. However, in comparison to standard aging there is an increase in elongation, which in Takata's study was attributed to a suppression of dynamic recovery during deformation and a modified dislocation distribution. Several authors[19–21] have also studied the effect of a two-step heat treatment where initial artificial aging was interrupted and then continued for long periods at a lower temperature (65 °C). This causes two different classes of phases/clusters/GP-zones (depending on the alloy system) to form, generating increased strength with no negative effects on ductility. In these studies, this is linked to an increased number of clusters forming at lower temperatures, as the main part of the bimodal distribution[19–21]. However, all of these heat treatments take several days or weeks.

The second way to produce a microstructure based on clusters which enables favourable combinations of strength and ductility is cyclic deformation of super-saturated age-hardenable alloys[17,22–24]. Cyclic deformation of aluminium alloys is thought to increase the excess vacancy concentration and thus to enable diffusion of solutes for cluster formation at room temperature[17].

The two processing routes discussed above illustrate that strengthening at low temperature to promote the formation of clusters can generate interesting properties. Although cyclic plasticity is a new and promising approach, to the best of the authors' knowledge no large-scale industrial application has so far been reported. Long-term annealing at low temperatures, known about for some time[19], has not yet attracted much attention in the industry, possibly due to investment in long-term heat treatments.

In this study, we describe a comparable fast heat treatment strategy that combines high strength and ductility. A combination of up-quenching (rapid heating combined with water quenching) and medium-temperature annealing purposes to form vacancies at high temperatures and retain them when cooled to lower temperatures suitable for cluster formation.

The following questions initially need to be addressed regarding the concept of up-quenching: (i) At what rate and to what extent do thermal vacancies form during up-quenching? (ii) What structural changes are caused by up-quenching if applied after an initial medium-temperature pre-annealing step? (iii) How does initial pre-annealing affect up-quenching's effectiveness? To answer these questions, in this study we illustrate and experimentally validate suitable process parameters for the design of an alternative processing route. Finally, we present a much quicker route to extensive cluster formation than seen in conventional aging treatments of aluminium alloys, leading to an improvement in strength with limited loss of ductility.

Results

Simulation-assisted design of vacancy-tuned aging treatments using up-quenching. To estimate how vacancy concentration develops during up-quenching and thereafter, thermo-kinetic simulations were conducted with the MatCalc 6.00 software package (further details on this simulation tool are found in the 'Methods' section)[25]. To calculate the equilibrium and non-equilibrium vacancy concentration the input of the following parameters was required: (i) the heating rate; (ii) the average grain size present; and (iii) the dislocation density (assumption 10^{-11} m^{-2} with a jog fraction of 0.02). Figure 1a shows the temperature profile of the aluminium sheets upon insertion into a metal bath (Bi57Sn43) at 250 °C. Reaching the target temperature takes roughly 2 s (after 1 s, a temperature of 215 °C is reached). From this an average heating rate of 130 K/s was calculated. Optical microscopy revealed an average grain size of about 50 µm (Fig. 1b). At 250 °C, as an example, it is calculated that a considerable number of vacancies (non-equilibrium) close to equilibrium will be formed after 10 s at designated sources—grain boundaries and dislocation jogs—and that the material will be equilibrated after ~15 s (Fig. 1c). Because up-quenching is performed after pre-annealing at 100 °C, the vacancy density equals the equilibrium value from 100 °C at the start of up-quenching. Due to heat transfer, the non-equilibrium vacancy density starts to increase only after 1 s. Figure 1d illustrates the combined heat

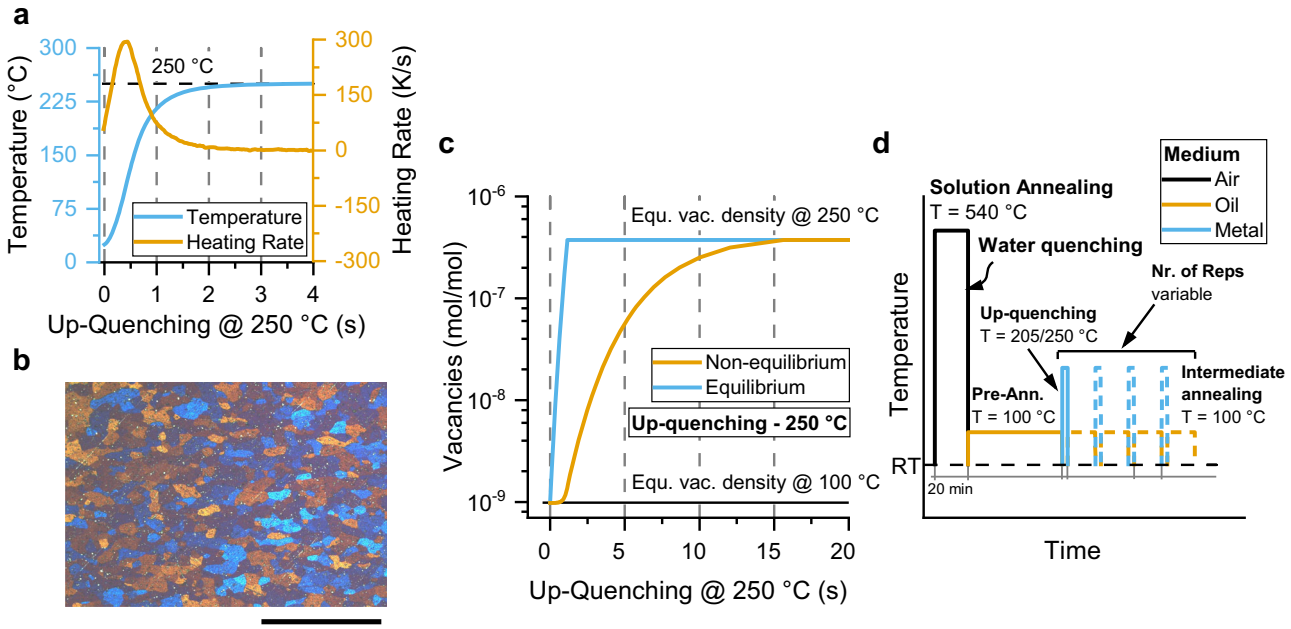

Fig. 1 Input parameters and thermo-kinetic simulations for the design of combined heat treatments using up-quenching. a Thermal profile of a 1.7-mm thick sheet upon immersion into a metal bath at 250 °C, measured with an embedded Type K thermocouple. This simulates up-quenching. **b** Grain structure of the commercial EN AW-6016 sheet used in T4 state (the scale bar corresponds to 500 µm). **c** Simulated vacancy evolution during up-quenching at 250 °C at a heating rate of 130 K/s with the grain boundary and dislocation jogs as the major vacancy sources. More than 10 s are required to generate a considerable number of vacancies (~75% of the equilibrium value). **d** Schematic illustration of the combined heat treatment.

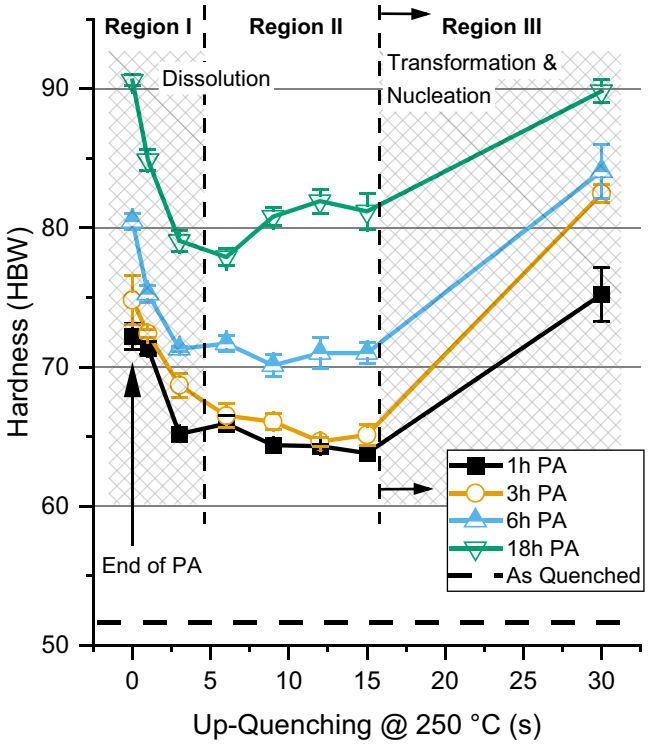

Fig. 2 Hardness evolution due to up-quenching after pre-annealing. Hardness measurements were performed following a single application of up-quenching at durations of 1–30 s at 250 °C to specimens pre-annealed (PA) for 1–18 h at 100 °C. The rapid drop in hardness within the first 3 s is associated with cluster dissolution, while the latter increase is linked to precipitation and transformation. The error bars for each hardness measurement were determined from at least five hardness indents and represent one standard deviation.

treatment developed. Solution annealing at 540 °C and water quenching are followed by pre-annealing at 100 °C, the aim being the formation of clusters (analogous to long-term aging at 100 °C) before the first up-quench is applied at 250 °C/205 °C. After each up-quenching step, intermediate annealing at 100 °C is carried out to deploy the increased vacancy density for continued cluster formation. A list of all time-temperature combinations applied can be found in the supplementary information (Supplementary Table 1).

Evaluation of the impact and effectiveness of up-quenching. Figure 2 shows the response of a commercial Al–Mg–Si sheet alloy pre-annealed at 100 °C for 1–18 h, followed by one up-quenching step at 250 °C (for the processing route see the solid line in Fig. 1d). As expected, at increasing pre-annealing duration the material exhibits increasing hardness values ranging from 72 Brinell hardness (HBW) (1 h) to 91 HBW (18 h). We attribute this to increased cluster formation (for interpretation details see the 'Discussion' section). When up-quenching at 250 °C is applied after pre-annealing at 100 °C, the hardness drops rapidly during the first seconds of up-quenching (region I), which we associate with a (partial) dissolution of initially formed clusters. However, there is still a significant gap between the hardness values after up-quenching and the values before pre-annealing is applied ("As-Quenched" in Fig. 2), implying an incomplete dissolution of clusters. For the longest up-quenching period examined (30 s) the hardness starts to increase again due to the formation of new hardening phases (region III). Region II is therefore characterized by an ambivalent process of cluster dissolution (predominantly seen in region I) and precipitation processes, which dominate in region III.

Figure 2 demonstrates that clusters dissolve rapidly (starting at 1 s) though only partially when subjected to up-quenching at 250 °C in pre-annealed alloys. The calculations in Fig. 1c suggest that the timescale for vacancies to be generated near the

equilibrium value is longer. To prove this for our alloy system, we tested the effectiveness of up-quenching treatments using natural aging, i.e. clustering at RT, as a marker for the vacancy content. Excess vacancies due to quenching from high temperatures, i.e. up-quenching, in addition to the necessary super-saturated solutes are well known as the driver of natural aging during RT storage[17,26–31]. For this reason, the hardness evolution of up-quenched samples upon natural aging was utilized to evaluate the potency of up-quenching. It is therefore assumed that the natural aging kinetics and the resulting hardness increase correlate with the vacancy density achieved at the up-quenching temperature (compare to Fig. 1c).

Figure 3a–d shows the natural aging behaviour of samples treated by pre-annealing at 100 °C and one up-quenching step at 250 °C. The solid lines represent the hardness increment of these combinations after one week of room temperature storage (natural aging). For comparison, the hatched lines depict the drop in hardness caused by up-quenching (depicted as an absolute value) starting from the pre-annealed hardness (values from Fig. 2). These values are assumed to be proportional to a (partial) dissolution due to the high annealing temperature and should thus allow an assessment of the freshly released quantity of dissolved solutes that are additionally available for natural aging.

In Fig. 3a–c (1–6 h of pre-annealing), an increase in natural aging is observed upon an increase in the dwell time of up-quenching. This behaviour is delayed if the pre-annealing time is extended. In general, we attribute this increased natural aging response when durations of up-quenching are increased to an increase in vacancy concentration, as predicted by the simulations in Fig. 1c. In contrast, up-quenching applied after 18 h of pre-annealing (Fig. 3d) prompts virtually no natural aging response. Potential explanations for this behaviour are given in the discussion.

Integration of up-quenching into multi-step heat treatment. With this information on the effectiveness of up-quenching especially after 1 and 3 h of pre-annealing (Fig. 3), we can now design treatments for enhanced cluster hardening which effectively involve a combination of high-temperature kinetics with low-temperature thermodynamics during intermediate annealing at 100 °C. For individual up-quenching parameters, two facts are important. On the one hand, up-quenching has to last long enough for vacancies to form sufficiently at high temperatures. The simulations from Fig. 1c, verified by experimental results in Fig. 3, indicate that for 250 °C roughly nine to twelve seconds seem adequate. On the other hand, up-quenching itself should not generate precipitation processes or a complete dissolution of previously formed clusters. A duration limit of 15 s seems suitable, as the hardness does not change much after a drop at the beginning of up-quenching (Fig. 2). For this reason, we chose 12 s at 250 °C as optimal. If the up-quenching temperature is lower (<250 °C), longer times must be selected, and vice versa.

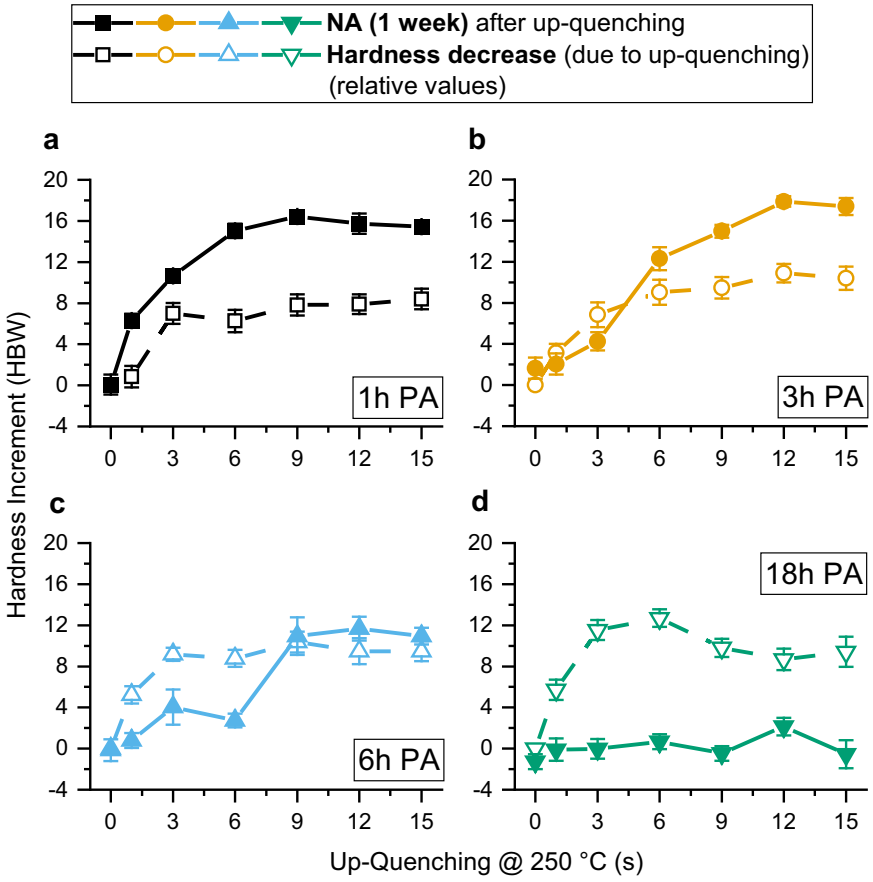

Fig. 3 Hardness increase after 1 week of natural aging following pre-annealing (PA) at 100 °C and up-quenching. The 1-week hardness increase is measured after pre-annealing for **a** 1 h, **b** 3 h, **c** 6 h and **d** 18 h, and the application of up-quenching for durations of 1–15 s at 250 °C (solid lines). For comparison, the hatched lines show the drop in hardness from the pre-annealed state due to up-quenching only (compare to Fig. 2), depicted as absolute values. Long up-quenching times can promote increased natural aging kinetics by generating equilibrium vacancies in line with Fig. 1c. The error bars for each hardness measurement were determined from at least five hardness indents and represent one standard deviation.

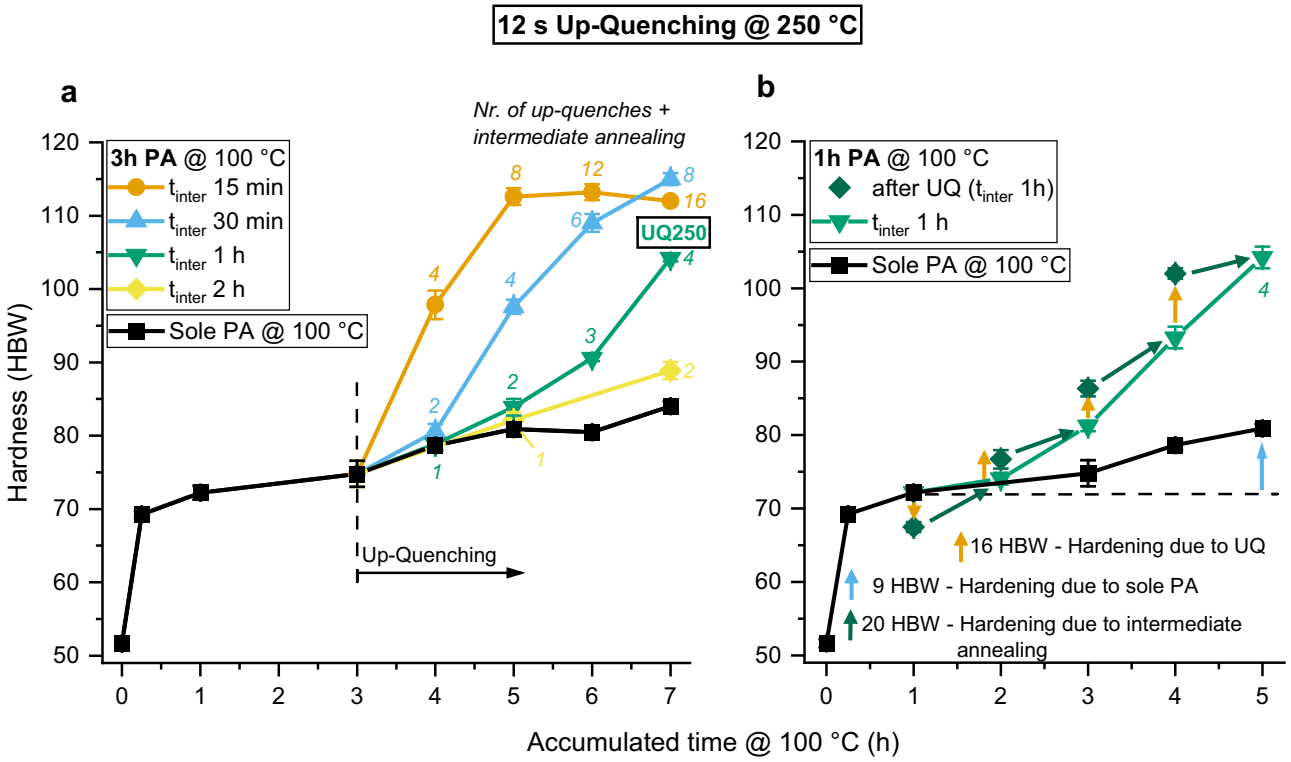

Fig. 4 Acceleration of hardening during annealing at 100 °C via up-quenching. a Pre-annealing (PA) (3 h; 100°C), up-quenching (12 s; 250 °C) and intermediate annealing (15 min to 2 h; 100 °C). Accumulated time stands for the total time at 100 °C (pre-annealing + t_{inter}). **b** Pre-annealing (PA) (1 h; 100 °C), up-quenching (12 s; 250 °C) and intermediate annealing (1 h; 100 °C). A gradual hardness evolution is shown in (**b**). The three numerical hardness values represent the total hardness increase triggered by the different treatments (illustrated by differently coloured arrows). Whereas hardness decreases due to up-quenching after 1 h, the second and every subsequent up-quenching cause a hardening increase (orange arrows, 16 HBW). Compared to just pre-annealing (blue arrow, 9 HBW), up-quenching causes hardening to double during the subsequent intermediate annealing steps at 100 °C (green arrows, 20 HBW). The error bars for each hardness measurement were determined from at least five hardness indents and represent one standard deviation.

During up-quenching it is desirable to repeatedly pump down thermal vacancies from elevated temperatures to accelerate clustering during annealing at 100 °C, which can generate the desired increase in strength without reduced elongation. We tested several combinations of pre-annealing and intermediate annealing (t_{inter}), as shown in Fig. 4a (according to the heat treatment scheme in Fig. 1d, solid + dashed line). Three hours of initial pre-annealing aims to fully exploit the beneficial state of high solute supersaturation and high excess vacancy density after quenching. Supplementary Fig. 1a indicates that a minimum of 1 h is needed before most of the quenched-in vacancies after solution annealing annihilate. This does not take into account formed clusters as traps in the simulation, which would further increase this time. Pre-annealing is followed by up-quenching (12 s at 250 °C). Then intermediate annealing takes place after each up-quench for 15 min to 2 h (t_{inter}, 100 °C). Supplementary Fig. 1b shows that excess vacancies are present for about 60 min after up-quenching during annealing at 100 °C, again without considering vacancies being trapped by clusters. The *x*-axis in Fig. 4a describes the total time during which the samples are annealed at 100 °C (pre-annealing-time + t_{inter}). Hardness increases slowly with time with pre-annealing at 100 °C only (black line). A combination with up-quenching generates accelerated hardening, which we associate primarily with faster cluster formation at 100 °C. Data from further parameter combinations, showing similar hardness evolution, can be found in the supplementary material (Supplementary Fig. 2).

Figure 4b depicts the hardness evolution step by step during the combined heat treatment. While Fig. 2 and the first green data point in Fig. 4b after 1 h of accumulated annealing time show clearly that hardness decreases after pre-annealing due to up-quenching at 250 °C, different characteristics are revealed during subsequent up-quenches. Hardness increases not only during intermediate annealing, but also during up-quenching itself starting from the second up-quenching cycle. It is obvious that during intermediate annealing at 100 °C, hardness increases in total (20 HBW) by double the amount generated by mere pre-annealing (9 HBW) over the same period of 1–5 h. This clearly demonstrates the positive effect that up-quenching has on aging kinetics at 100 °C. Nevertheless, any further up-quenches after the first also themselves contribute, in an increasing manner, to the total hardness increase (for 4 up-quenching cycles the contribution is 16 HBW in total). In summary, accelerating hardening depends on how many times up-quenching is repeated, in other words, on the pumping of vacancies into the super-saturated solid solution. Yet it seems that there is a threshold to the number of beneficial up-quenching cycles.

As mentioned in the introduction, it has been shown that very long—and potentially economically less attractive—aging times at 100 °C generate an exceptionally good combination of strength and ductility in 6xxx-alloys[16]. In this study, we repeated this procedure using a 6xxx-alloy and evaluated possible up-quenching strategies to shorten the aging times required to reach sufficient strength.

Figure 5a shows stress–strain curves for two different heat treatments. The hatched line represents a sample that was annealed only at 100 °C for 168 h. Such long-term annealing generates a yield strength of 220 MPa with still-high elongation to fracture (28%) corresponding to the beneficial structure formed[9,12]. The resulting parameter pair was then used as a test case to investigate whether our strategy can be used to produce the desirable material state within reasonable time scales.

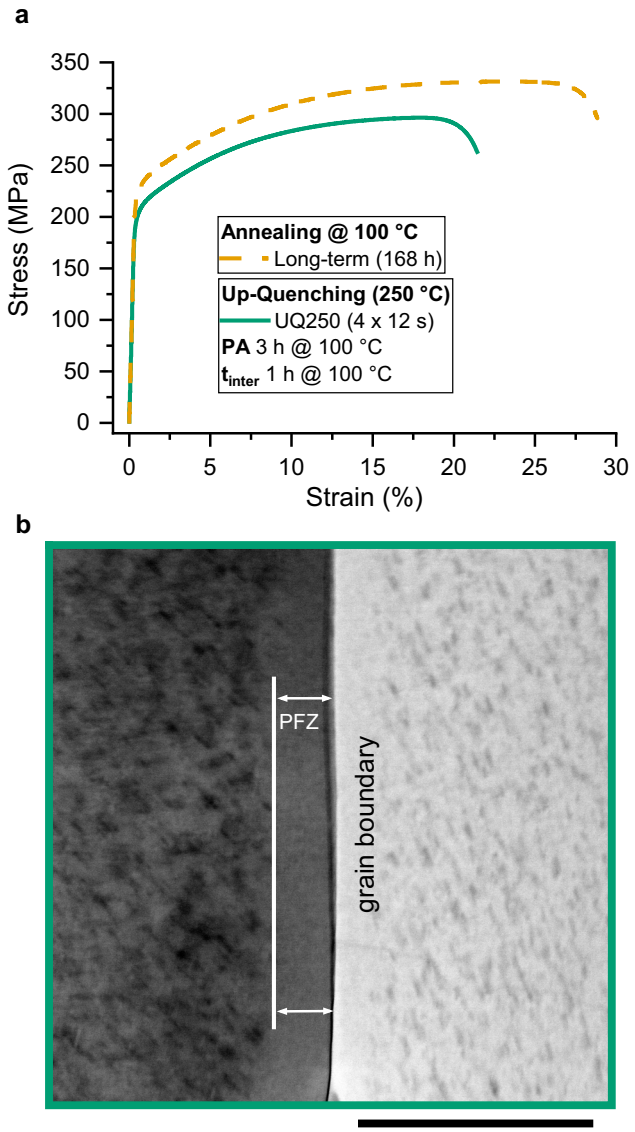

Fig. 5 Stress–strain diagram and corresponding microstructure of UQ250 examined by STEM. a Stress–strain curves resulting from up-quenching strategy UQ250 and long-term medium-temperature annealing. **b** LAADF-STEM micrograph of UQ250 shows a pronounced precipitate-free zone (PFZ) along a representative grain boundary. The scale bar corresponds to 150 nm. "PA" stands for pre-annealing.

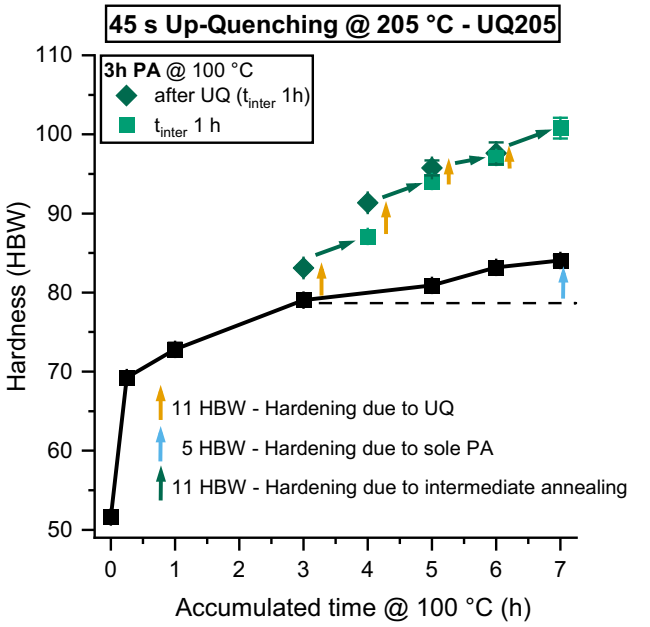

Fig. 6 Acceleration of hardening during annealing at 100 °C via up-quenching at 205 °C. A gradual hardness evolution upon up-quenching the samples at 205 °C for 45 s and 1 h of intermediate annealing after 3 h of pre-annealing is shown. The three numerical hardness values represent the total hardness increase triggered by the different treatments (illustrated by differently coloured arrows). Due to the decreased up-quenching-temperature of 205 °C, hardness increases due to each up-quenching (orange arrows, 11 HBW). However, compared to sole pre-annealing (blue arrow, 5 HBW), up-quenching causes increased hardening during the subsequent intermediate annealing steps (green arrows, 11 HBW). "PA" stands for pre-annealing. The error bars for each hardness measurement were determined from at least five hardness indents and represent one standard deviation.

From the combinations tested in Fig. 4 and Supplementary Fig. 2 using 250 °C as the up-quenching temperature, various heat treatment states were picked for tensile testing. The combination showing the highest elongation is depicted in Fig. 5a as an example. It consists of four up-quenches to 250 °C with 3 h of pre-annealing and 1 h of intermediate annealing (in total 7 h; this heat treatment is denoted in the following as UQ250), and generates a yield strength of 200 MPa (Fig. 5a). However, compared to our test case involving long-term annealing at 100 °C the fracture elongation is significantly lower, and the good combination seen in the material annealed at long-term medium temperatures is not reached when up-quenching to 250 °C is applied. While the high up-quenching temperature of 250 °C is optimal for creating thermal vacancies, high temperatures may create wider precipitate-free zones, decreasing ductility[32,33]. Scanning transmission electron microscopy (STEM) results, shown in Fig. 5b, revealed a precipitate-free zone width of 34 ± 3 nm next to the grain boundary after UQ250. The first shot treatment using 250 °C as the up-quenching temperature also transformed some clusters into metastable precipitates, which reduces the benefits of cluster hardening (see also the BF-TEM image in Supplementary Fig. 3a).

Adjustment of up-quenching parameters for enhanced ductility. For this reason, we decided to investigate a similar treatment (with the same pre-annealing and t_{inter}), but with a reduced up-quenching temperature of 205 °C. Our intention was to mitigate these negative effects while still generating a vacancy concentration that is two orders of magnitude higher than when annealing only at 100 °C. According to our simulations, for the alloy we used 45 s are enough to achieve a vacancy concentration near-equilibrium density at 205 °C (see Supplementary Fig. 4a for more details). Here, in contrast to 250 °C, hardness increases even during the first up-quench, as depicted in Supplementary Fig. 4b and Fig. 6. This implies that clusters formed at 100 °C do not dissolve at 205 °C. Similarly to UQ250, every subsequent up-quench at 205 °C also increases hardness, but in addition increases hardness during subsequent intermediate annealing at 100 °C (see Fig. 6). Because the vacancy generation at 205 °C is not as extensive as that at 250 °C, hardening during intermediate annealing is reduced if we compare Fig. 4b with Fig. 6, but the concept still applies.

Taking another look at tensile testing, up-quenching treatment at 205 °C (denoted as UQ205 in the following; 4 up-quenches to 205 °C with 3 h of pre-annealing and 1 h of intermediate

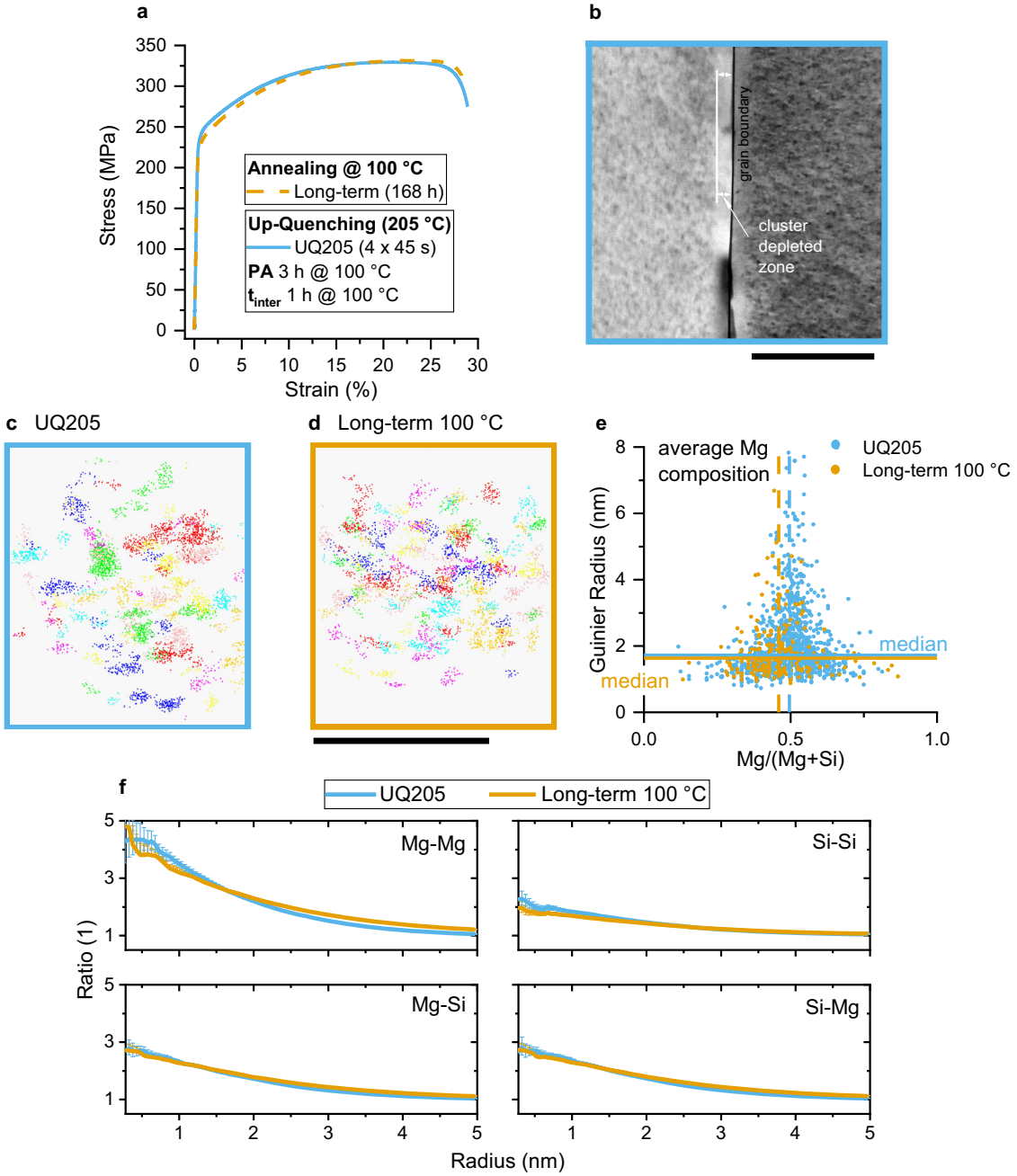

Fig. 7 Stress–strain curves resulting from up-quenching strategy UQ205 plus long-term annealing and corresponding microstructure. a Stress–strain diagram. **b** LAADF-STEM micrograph of a representative grain boundary for UQ205 (the scale bar corresponds to 150 nm). **c**, **d** Depiction of all solutes that are incorporated into clusters in an equally large cylinder cut from the whole sample volume for UQ205 (**c**) and for long-term annealing (**d**) measured via APT (the scale bar corresponds to 30 nm for (**c**) and (**d**)). **e** Size of clusters (Guinier radius) in relation to the Mg-content of each cluster from APT. **f** Spatial position analysis of solute atoms from APT. Up-quenching at adequate temperate (205 °C) accelerates cluster hardening and, within 7 h, generates mechanical properties and microstructure comparable to those produced by long-term annealing at 100 °C for 168 h. "PA" stands for pre-annealing. Error bar boundaries are calculated using the mean value of the randomized radial distribution function and its standard deviation (for further information please see ref. [35]).

annealing, in total 7 h) now shows results as good as those achieved after 168 h of long-term medium-temperature annealing treatment (Fig. 7a). This accounts for only four percent of the time needed without up-quenching. Figure 7b also reveals a decrease in the solute depleted zone around the grain boundary to 15 ± 3 nm compared to UQ250 (Fig. 5b).

To obtain concise evidence on the microstructure of the UQ205 sample (blue curve in Fig. 7a), we used atom probe tomography (APT) (Fig. 7c–f). For comparison, APT was also applied to the long-term (168 h) annealed sample (dashed orange curve in Fig. 7a). The solutes (Mg, Si and Cu) incorporated in clusters are depicted in Fig. 7c for UQ205 and in Fig. 7d for long-term annealing. Each cluster is represented in a different colour. In both samples, the clusters are evenly distributed throughout the volume shown. Consequently, the cluster number densities for UQ205 ($2.55 \times 10^{24}\,m^{-3}$) and for long-term annealing ($2.48 \times 10^{24}\,m^{-3}$) are comparable. The degree of solutes in clusters is high and is nearly the same for both samples (see

Table 1 Chemical analysis of the matrix and clusters found via APT.

(atom-%)	Up-Quenching (UQ205)			Long-term 168 h (100 °C)		
	Cu	Mg	Si	Cu	Mg	Si
Overall composition	0.068	0.733	1.148	0.081	0.621	1.066
Cluster composition	0.162	15.676	15.878	0.207	13.929	16.532
Matrix composition without clusters	0.067	0.536	0.954	0.080	0.422	0.835
Fraction of solutes in clusters (%)	3.1	27.8	18.0	3.7	33.0	22.8

Chemical characteristics of clusters and matrix for UQ205 and long-term annealing measured by APT.

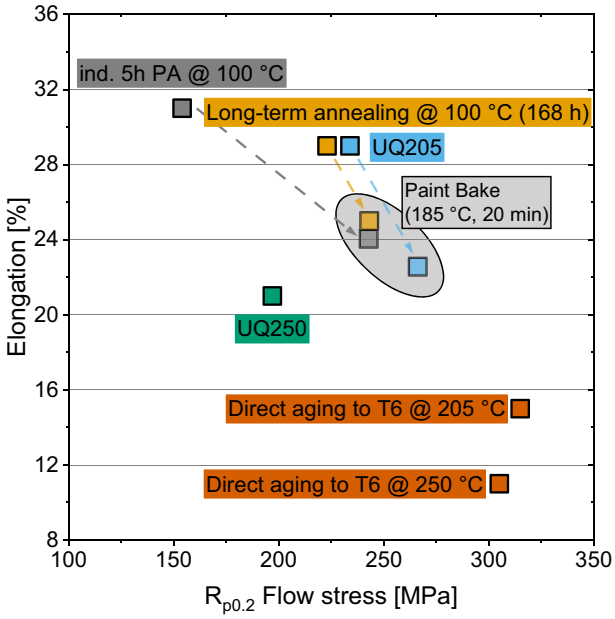

Fig. 8 Comparison of elongation vs. yield strength of the Al–Mg–Si alloy tested after different heat treatments. Direct aging to T6 at 205 and 250 °C generates low elongation values, and UQ250 shows an insufficient combination of low elongation and low strength. Of all the specimens primarily strengthened at 100 °C (ind. 5 h pre-annealing, long-term annealing at 100 °C and UQ205), UQ205 incorporates the greatest strength at comparable elongation values. After industrially typical artificial aging (paint bake, 185 °C, 20 min), indicated by a grey box/dashed arrows for the concerning heat treatment, UQ205 shows the highest strength and elongation values.

Table 1: fraction of solutes in clusters). The Mg- and Si-content of all clusters in relation to their respective Guinier radii is plotted in Fig. 7e. Every dot stands for one measured cluster (note that the total number of atoms measured via APT was different, which explains the higher number of blue data points in Fig. 7e). For both treatments the majority of clusters can be found in the middle of the diagram, indicating an Mg-share of between 0.33 and 0.66, which is characteristic of clusters formed at around 100 °C[8,34]. The largest share is seen at small sizes (median of all clusters: 1.7 nm for UQ205, 1.6 nm for long-term annealing), and there is no big discrepancy in the average Mg composition of all clusters detected. Figure 7f represents the ratio of the cumulative sums of the radial distribution for all possible Mg–Si interactions in relation to a simulated randomized distribution. Hence every value above 1 indicates clustering (see ref. [35] for more details on this method). In this respect, strong interactions are present for all combinations tested (Mg–Mg, Mg–Si, Si–Mg and Si–Si) indicating cluster formation (deviations in the individual RDF ratios are primarily attributed to the total solute content of Mg and Si). The important fact is that these RDF plots reveal no discrepancy between the heat treatment UQ205 and long-term annealing. These results strongly support our expectation of accelerated cluster formation after up-quenching at 205 °C, generating an outcome similar to that of long-term annealing; see the tensile testing results in Fig. 7a.

Comparison of the combined heat treatment to conventional aging parameters. Figure 8, finally, presents an elongation-tensile strength chart for various heat treatments applied to the Al–Mg–Si alloy examined here. In the chart we compare conditions such as industrially common pre-aging (5 h, 100 °C) and long-term annealing with/without a paint-bake simulation (185 °C, 20 min), and direct artificial aging to T6 at the applied up-quenching temperatures, to the results from up-quenching (UQ250 and UQ205). We also added a paint bake to UQ205. As discussed above, UQ250 shows insufficient elongation. Direct artificial aging to T6 at 205 and 250 °C results in good strength, but relatively low elongation. The industrially common pre-aged and paint-baked condition performs well, but long-term annealing and especially UQ205 show significantly higher strength values at only slightly reduced elongation. A paint bake of UQ205 further increases strength at the expense of elongation, but the combination is still interesting.

Discussion

Pre-annealing and up-quenching have a major impact on hardness evolution through cluster formation and dissolution. This result is discussed below and put into context in terms of the existing literature.

After solution annealing and quenching, pre-annealing leads to increasing hardness values due to increasing numbers of clusters[14], as seen in Fig. 2. After this, up-quenching at 250 °C causes a lowering of the hardness values, probably because the temperature is above the solvus temperature of clusters[9,36]. After this initial drop, hardness keeps stagnating significantly above the low as-quenched value, which indicates either that complete dissolution of clusters does not occur, or that hardness is already being generated by cluster growth or by the formation of metastable elongated precipitates. An incomplete dissolution of clusters formed at RT after a short heat treatment at 250 °C was also seen elsewhere[37,38], but those results indicate that clusters formed at room temperature dissolve to a larger extent at 250 °C, i.e. hardness can drop almost down to the start value. Thus, it seems that clusters formed at higher temperatures (100 °C) are thermally more stable or transform more easily into other hardening phases at 250 °C. At the longest up-quenching times examined in Fig. 2 ($t > 15$ s) an increase in hardness is seen, which we associate with a transformation of clusters predominantly into metastable strengthening phases, or individual nucleation of the latter[39]. Typically, a vast transformation of clusters formed during industrially applied pre-aging treatments at around 100 °C into

other metastable phases like β″ takes place during artificial aging around 180 °C[40].

Natural aging behaviour after a single up-quench shows different hardness evolutions, depending on both the prior pre-annealing time and the up-quenching duration itself (Fig. 3). Generally, after 1–6 h of pre-annealing (Fig. 3a–c) increasing dwell times for up-quenching lead to an increase in natural aging (as also seen in our previous work[41]). Taking the simulations from Fig. 1c into consideration, longer up-quenching ≥10 is thought to generate a considerable number of vacancies near the equilibrium value. The saturation of the natural aging value at 10–15 s also accords with the time predicted for reaching the equilibrium vacancy concentration. However, the situation observed is very complex due to unclear dislocation characteristics and an interaction of clusters with vacancies, which is not considered in the simulations. Consequently the results of simulations must be approached with some caution.

In addition to the general trend mentioned above, Fig. 3a inspires two major observations. First, the hardness generated upon natural aging after pre-annealing and up-quenching is twice as high as what we can expect from the solutes released by dissolving clusters only. This indicates only a minor reduction of supersaturation after short pre-annealing (as also seen elsewhere[42,43]) and significant vacancy generation upon up-quenching, boosting natural aging. The growth of clusters that survive up-quenching during natural aging may also generate a strong increase in hardness, as it has been shown that the growth of clusters has a greater influence on the increase in hardness than does an increase in the number density during the natural aging process[44].

Second, a natural aging response directly follows a one-second up-quench for the one sample which was pre-annealed for 1 h only. Due to heating (after 1 s of up-quenching 215 °C is reached), only a low number of thermal equilibrium vacancies form in the shortest time investigated (see also simulations in Fig. 1c). One reason for the distinct natural aging here might be a release of vacancies from clusters formed after 1 h of pre-annealing at 100 °C. It is known that vacancies play a crucial role in the formation of clusters by assisting the diffusion of solutes[28]. Once formed, vacancies are thought to be incorporated into clusters due to a compensation of strain energy[45] or attractive binding[32,46]. However, recent investigations indicate that no or only a minor number of vacancies (below the equilibrium vacancy density of 250 °C) are released if a 250 °C-spike is applied after 2 weeks of natural aging[37]. Thus a vacancy release from clusters presents an interesting approach which cannot, however, be proven here. The high supersaturation which still remains after 1 h of pre-annealing is considered a further reason for the boosting of the natural aging response observed here.

In contrast, Fig. 3b and c shows that such very brief up-quenching does not promote natural aging, although clusters from pre-annealing dissolve (hatched line is above the solid one for short up-quenching durations). Instead, the timescale for vacancy formation simulated in Fig. 1c is observed in the natural aging response. We thus suggest that pre-annealing at 100 °C may produce different types of clustering state as the annealing time increases, i.e. clusters both with and without incorporated vacancies. According to our experimental data it takes roughly 3–6 h for clusters to shed vacancies upon pre-annealing at 100 °C, which corresponds to pure annihilation of excess vacancies at 100 °C after solution annealing at 540 °C (around 3 h according to the FSAK model; see Supplementary Fig. 1a).

It can be seen that increasing the duration of pre-annealing decreases the maximum hardness increment achieved via natural aging. This effect may have two causes: (i) a reduced remaining solute supersaturation; or (ii) more developed clusters (indicated by increased hardness values after longer pre-annealing; see Fig. 2). It has been shown that even after 24 h of aging at 90 °C, large amounts of Si and Mg remain in solid solution[26]. Moreover, from cyclic deformation, causing a continuous supply of vacancies, it is known that cluster formation continues until a T6-like strength is reached even at room temperature. Thus option (i) is less likely. Interestingly, the maximum absolute drop in hardness immediately after up-quenching is in the range of 8–13 HBW for all pre-annealing times (see hatched lines in Fig. 3), although hardness rises by 19 HBW going from 1 to 18 h of pre-annealing. Accordingly, the number of undissolved, surviving clusters increases after up-quenching at longer pre-annealing-times. According to Zurob and Seyedrezai[28], an increased trap strength of clusters is favoured by enlarged cluster sizes and greater number density. Hence, clusters after long pre-annealing may decrease the mobility of vacancies created via up-quenching at RT, slowing down the NA response. However, the available experimental data allow only indirect conclusions about the incorporation of vacancies in clusters. Nevertheless, the results from hardness testing enable an interpretation of the formation of clusters at elevated temperatures, as typically used for pre-aging treatments[41,47].

During the course of the combined heat treatment, various hardness changes are observed due to the application of an up-quench. Whereas the first up-quench at 250 °C leads to a small hardness decrease (Figs. 2 and 4b), every subsequent up-quench leads to hardening itself. Here, increasing cluster growth during up-quenching or the formation of metastable, coarse phases seem plausible. In contrast, up-quenching at 205 °C never leads to any hardness decrease (Supplementary Fig. 4b and Fig. 6), indicating no cluster dissolution. It seems that clusters tend rather to grow from the first up-quench onwards, which was also reported by Serizawa et al.[48] to happen at 180 °C. In this respect, a decreased dissolution tendency is also seen for clusters formed at RT when reducing the annealing temperature from 250 to 210 °C[38], similarly to our case.

Besides the formation of coarse metastable precipitates (Fig. 5b and Supplementary Fig. 3a) due to up-quenching at high temperatures such as 250 °C, the formation of PFZs may also mitigate the benefits of this heat treatment concept. It has been shown that aging at low temperatures generates very narrow PFZs, causing preferential material behaviour that involves high strength and high elongation[32,33]. If we compare the widths of the solute depleted zones of UQ250 (34 nm) to UQ205 (15 nm), worse mechanical properties for the 250 °C up-quenching procedure (Figs. 5a and 7a) can be attributed to this, although both up-quenching treatments show typical widths compared to standard artificial aging procedures (20–35 nm after water quenching and aging at 190 °C to T6, AA6156[49]). This shows that 4 × 12 s of aging at 250 °C (4 × up-quenching) are enough to cause the microstructure to deteriorate to such an extent that this cannot be ameliorated by aging again at 100 °C, which should hinder the formation of PFZs. In this context it is surprising that a fresh supply of vacancies, which are thought to be primarily formed at grain boundaries, due to up-quenching does not inevitably help to suppress the formation of PFZs. However, a reduced up-quenching temperature successfully limits PFZ formation and enables extensive cluster formation, improving strength with limited loss of ductility (Fig. 7).

In conclusion, our experimental results largely support the theoretical concept proposed for repeatedly pumping vacancies to a super-saturated alloy via up-quenching. By this means we were able to accelerate diffusion-controlled reactions at medium temperatures (such as 100 °C) and enable transformations which are not usually accessible at feasible time scales. In this study the concept was applied to a commercial Al–Mg–Si alloy to generate

cluster hardening, which is a promising strengthening strategy but unfortunately shows slow kinetics when common isothermal heat treatments are used. Here we successfully demonstrated such a strategy at much shorter time scales. The required processing time was reduced by 96% compared to the known long-term annealing procedure for generating distinct cluster hardening, while it still achieved a similar favourable strength/ductility combination in a comparable microstructure, down to the nanometre scale.

Extending the up-quenching strategy to various other types of alloy from the important Al–Mg–Si class seems straightforward, because determining process parameters such as temperature and soaking times can be roughly simulated using thermo-kinetic calculations. In terms of industrial application, however, it is essential to consider that the adjustable boundary conditions (temperature, time, heating and cooling rate) are not the only factors which alter the effectiveness of the treatment. The grain size of the alloy used, which strongly determines the amount of vacancy generation sites, theoretically has a massive influence; this is demonstrated in Supplementary Fig. 5. In addition to grain size, other microstructural elements also control vacancy generation kinetics (interfaces/free surfaces such as incoherent particles[50,51]) and need to be taken into account when designing the heat treatment. The potential to adjust parameters, coupled with the fact that the required technical equipment (i.e. infrared heaters and quenching bars) is already in use in the commercial production of aluminium sheets, mean that large-scale industrial application seems feasible. Moreover, in thin automotive sheets rather small thermal gradients are expected during up-quenching, due to the high thermal conductivity of aluminium[1].

Regarding the interaction of clusters with vacancies, the results available (especially from hardness testing) indicate an interaction and varying behaviour depending on the heat treatment applied. Because the focus of this study was to investigate appropriate process parameters for our up-quenching concept, a more in-depth discussion would require more experimental data, probably from applying further characterization methods such as PALS, DSC or electrical resistivity measurements to pure ternary systems. Nevertheless, we are assured that our indirect interpretations can initiate further investigations and contribute to the long-standing academic discussion of cluster development in the field of Al–Mg–Si alloys[37,52]. Finally, the study again demonstrates the complexity and potential involved in manipulating such systems.

To end, because cluster hardening time scales can be manipulated, up-quenching strategies may also be applicable to other types of commercial aluminium alloy. In general, the solute clustering process is not usually limited by the supersaturation of solutes, but gets kinetically stuck when excess vacancies are annihilated[27] or bound in metastable structures or clusters[28,53]. The repeated transfer of vacancies to such systems by up-quenching may boost the technological importance of and research in this field. Because kinetics is rendered "transferable" from one region to another, up-quenching broadens the range of possibilities. It facilitates a rearrangement of time-temperature-transition diagrams, and offers a further degree of freedom for any alloy featuring phase transitions controlled by substitutional diffusion, thus circumventing previous limitations on kinetics.

Methods

Material and experimental method. Commercial Al–Mg–Si sheets (Al-0.65Mg-1.16Si-0.17Cu, wt%) of 1.7-mm thickness in cold rolled condition were used as material. All heat treatments applied started with solution annealing (circulation air furnace, Nabertherm N60/85 SHA) at 540 °C for 20 min. After water quenching, the samples were transferred immediately to an oil bath (Lauda Proline P26) at 100 °C for pre-annealing for durations of between 15 min and 18 h. Afterwards, depending on the desired parameter combinations, different numbers of up-quenching repetitions (1–30 s, 205/250 °C) were conducted in a metal bath consisting of Bi57Sn43 to ensure fast heat transfer. The temperature was controlled by means of a Pt100 thermocouple inserted directly into the liquid metal bath. After each up-quench the samples were annealed in an oil bath at 100 °C for between 15 min and 2 h (intermediate annealing). Each single processing step concluded with water quenching. A schematic illustration is found in Fig. 1d. Supplementary Table 1 lists all processing parameters applied in each individual figure.

Mechanical testing. An EMCO-Test M4 device was used (HBW 2.5/62.5) for hardness testing. Five individual indents were made for one hardness value. A maximum standard deviation of 2 HBW was undershot. Uniaxial tensile testing was performed on a testing machine (Zwick/Roell) with a 50 kN load cell. Specimens were tested transverse to rolling direction with a gauge length of 45 mm. Three individual specimens were tested to derive one set of mechanical parameters.

Grain size evaluation. Optical microscopy (Zeiss Axio Imager M1m) was deployed for grain size evaluation (line intersection method). Optical micrographs of the alloy, etched with Barker's solution, were examined using polarized light.

Transmission electron microscopy (TEM). LAADF-STEM and BF-TEM measurements were performed using a Thermo Scientific^{TM} Talos F200X G2. 200 kV was the acceleration voltage. In all, 3-mm disc specimens were prepared via a standard route which consisted of grinding and electrolytic polishing with HNO_3 in methanol (1:3) at −20 °C and 15 V. A minimum of 13 grain boundaries were evaluated for both samples to analyze the PFZs.

Atom probe tomography (APT) sample preparation and measurement. Blanks ($0.7 \times 0.7 \times 20$ mm^3) were cut from undeformed parts of tensile testing specimens (UQ205; long-term annealing at 100 °C). Two-step electro-polishing was applied for sample production (first step 25% HNO_3 in methanol and second step 2% $HClO_4$ in 2-butoxyethanol). The samples were run in voltage mode with a pulse fraction of 20%, a frequency of 200 kHz and a detection rate of 1% at a temperature of 30 K on a LEAP 3000 X HR. The number of atoms detected was 20×10^6 for the UQ205 sample and 2.6×10^6 for the long-term annealed sample.

APT data analysis. The $^{24}Mg^{2+}$, $^{25}Mg^{2+}$, $^{26}Mg^{2+}$; $^{28}Si^{2+}$, $^{29}Si^{2+}$, $^{30}Si^{2+}$; $^{24}Mg^{+}$, $^{25}Mg^{+}$, $^{26}Mg^{+}$; and $^{63}Cu^{+}$, $^{65}Cu^{+}$ peaks were used for APT solute analysis. The reconstruction was created by calibrating the field factor k_f with the interlayer spacing observed and the image compression factor with the angles of chosen poles[54] observed within the commercial programme IVAS 3.6.12.

The cluster search was executed based on a threshold density calculated via Voronoi volume[55] for Mg and Si atoms as core atoms. The surface of a cluster was identified by the built-in MATLAB^{TM} "alphaShape" function with the Mg and Si atoms identified from the cluster search. All the atoms of a cluster, i.e. also the non-core atoms, were identified by finding atoms which are located within a surface defined for each cluster by the built-in "inHull"[56] function. Based on all the atomic positions found for each cluster, the Guinier radius was calculated according to Eqs. (1) and (2)[57].

$$s = \mathrm{Mean}([x_i, y_i, z_i]) \tag{1}$$

$$r_G = \sqrt{\frac{5}{3}\left(\sum_i (x_i - s_x)^2 + (y_i - s_y)^2 + (z_i - s_y)^2\right)} \tag{2}$$

Al, AlH_1 and AlH_2 are counted as Al; only Cu, Mg and Si atoms are counted for composition calculation.

The formalism described in refs. [35,58] was used for the radial distribution function analysis. The ratio of the experimental to a random comparator radial distribution function, in cumulative summed form, was used as a measure for non-randomness, e.g. clustering, of the spatial distribution of solute elements. Pair interactions (X–Y) are labelled such that X represents the solute atoms searched for (target) in the vicinity of Y solute atoms. Physically meaningless values for a radius below 0.28 are neglected, but information is still preserved due to use of the cumulative form.

For an overview of the clusters detected, a cylindrical volume ($40 \times 40 \times 40$ nm) of the whole datasets was used for UQ205 (Fig. 7c) and for long-term annealing (Fig. 7d). The Guinier radius over the Mg-composition scatter plot in Fig. 7e was calculated for all clusters detected. The RDF calculations in Fig. 7f were performed using cylindrical regions of interest from both samples, with cylindrical-like sizes of $20 \times 20 \times 50$ nm.

Thermo-kinetic simulations. MatCalc 6.00[25] software was used to perform thermo-kinetic simulations of vacancy evolution during up-quenching (Fig. 1c, Supplementary Figs. 1, 4a and 5). Using the FSAK model[50,59], both the annihilation and the generation of structural vacancies on idealized microstructural sources such as grain boundaries and dislocation jogs can be predicted. In this study, grain boundaries and dislocation jogs were considered. A grain size of 50 µm (for Fig. 1c, Supplementary Figs. 1 and 4a) and an equilibrium dislocation density of 10^{11} m^{-2}

(according to Dumitraschkewitz et al.[35], Fischer et al.[50] and Pogatscher et al.[60]) (Fig. 1c, Supplementary Figs. 1, 4a and 5) with a jog fraction of 0.02 were used as input parameters. The remaining parameters were chosen as follows: jog fraction on Frank loops 0.2, Frank loop nucleation constant 0, Frank loop interfacial energy 1, effective loop-line energy 0.5 Gb^2, excess vacancy efficiency 1. Applications of this vacancy model can be found in various references[35,60,61].

Data availability

The datasets generated and/or analyzed during this study are available at https://doi.org/10.17632/fggxfhnv6b.1.

Received: 21 July 2020; Accepted: 10 May 2021;
Published online: 07 June 2021

References

1. Ostermann, F. *Anwendungstechnologie Aluminium* (Springer-Verlag Berlin Heidelberg, 2014).
2. Wilm, A. German patent DRP 244554 (1906).
3. Wilm, A. Physikalisch-metallurgische Untersuchungen über magnesiumhaltige Aluminiumlegierungen. *Metallurgie* **8**, 225 (1911).
4. Vasudévan, A. K. & Doherty, R. D. Grain boundary ductile fracture in precipitation hardened aluminum alloys. *Acta Metall.* **35**, 1193–1219 (1987).
5. da Costa Teixeira, J. et al. On the strengthening response of aluminum alloys containing shear-resistant plate-shaped precipitates. *Acta Mater.* **56**, 6109–6122 (2008).
6. da Costa Teixeira, J., Bourgeois, L., Sinclair, C. W. & Hutchinson, C. R. The effect of shear-resistant, plate-shaped precipitates on the work hardening of Al alloys: towards a prediction of the strength–elongation correlation. *Acta Mater.* **57**, 6075–6089 (2009).
7. Kelly, A. & Nicholson, R. B. Precipitation hardening. *Progr. Mater. Sci.* **10**, 149–391 (1964).
8. Dumitraschkewitz, P., Gerstl, S. S. A., Stephenson, L. T., Uggowitzer, P. J. & Pogatscher, S. Clustering in age-hardenable aluminum alloys. *Adv. Eng. Mater.* **20**, 1800255 (2018).
9. Starink, M. J., Cao, L. F. & Rometsch, P. A. A model for the thermodynamics of and strengthening due to co-clusters in Al–Mg–Si-based alloys. *Acta Mater.* **60**, 4194–4207 (2012).
10. Ardell, A. J. Precipitation hardening. *Metall. Trans. A* **16**, 2131–2165 (1985).
11. Nembach, E. Precipitation hardening caused by a difference in shear modulus between particle and matrix. *Phys. Stat. Sol.* **78**, 571–581 (1983).
12. Starink, M. J. & Wang, S. C. The thermodynamics of and strengthening due to co-clusters: general theory and application to the case of Al–Cu–Mg alloys. *Acta Mater.* **57**, 2376–2389 (2009).
13. Li, H. & Liu, W. Nanoprecipitates and their strengthening behavior in Al-Mg-Si alloy during the aging process. *Metall. Mater. Trans. A* **48**, 1990–1998 (2017).
14. Noseda Grau, V., Cuniberti, A., Tolley, A., Castro Riglos, V. & Stipcich, M. Solute clustering behavior between 293K and 373K in a 6082 aluminum alloy. *J. Alloys Compd.* **684**, 481–487 (2016).
15. Chen, Y., Weyland, M. & Hutchinson, C. R. The effect of interrupted aging on the yield strength and uniform elongation of precipitation-hardened Al alloys. *Acta Mater.* **61**, 5877–5894 (2013).
16. Takata, K. et al. Improvement of strength–elongation balance of Al–Mg–Si sheet alloy by utilising Mg–Si cluster and its proposed mechanism. *Mater. Trans.* **58**, 728–733 (2017).
17. Sun, W. et al. Precipitation strengthening of aluminum alloys by room-temperature cyclic plasticity. *Science* **363**, 972–975 (2019).
18. Zhang, Q., Zhu, Y., Gao, X., Wu, Y. & Hutchinson, C. Training high-strength aluminum alloys to withstand fatigue. *Nat. Commun.* **11**, https://doi.org/10.1038/s41467-020-19071-7 (2020).
19. Lumley, R. N., Polmear, I. J. & Morton, A. J. Interrupted aging and secondary precipitation in aluminium alloys. *Mater. Sci. Tech.* **19**, 1483–1490 (2003).
20. Lumley, R. N., Polmear, I. J. & Morton, A. J. Development of mechanical properties during secondary aging in aluminium alloys. *Mater. Sci. Tech.* **21**, 1025–1032 (2005).
21. Takata, K. et al. Effect of two-step aging on cluster formation in Al–Mg–Si alloys. *Mater. Trans.* **55**, 885–891 (2014).
22. Han, W. Z., Chen, Y., Vinogradov, A. & Hutchinson, C. R. Dynamic precipitation during cyclic deformation of an underaged Al–Cu alloy. *Mat. Sci. Eng. A* **528**, 7410–7416 (2011).
23. Deschamps, A., Fribourg, G., Bréchet, Y., Chemin, J. L. & Hutchinson, C. R. In situ evaluation of dynamic precipitation during plastic straining of an Al–Zn–Mg–Cu alloy. *Acta Mater.* **60**, 1905–1916 (2012).
24. Hutchinson, C. R., Geuser, F. D., Chen, Y. & Deschamps, A. Quantitative measurements of dynamic precipitation during fatigue of an Al–Zn–Mg–(Cu) alloy using small-angle X-ray scattering. *Acta Mater.* **74**, 96–109 (2014).
25. MatCalc software package for computer simulation of phase transformation and microstructure evolution in metallic systems. www.matcalc-engineering.com.
26. Engler, O., Marioara, C. D., Aruga, Y., Kozuka, M. & Myhr, O. R. Effect of natural ageing or pre-ageing on the evolution of precipitate structure and strength during age hardening of Al–Mg–Si alloy AA 6016. *Mat. Sci. Eng. A* **759**, 520–529 (2019).
27. Banhart, J. et al. Natural aging in Al-Mg-Si alloys—a process of unexpected complexity. *Adv. Eng. Mater.* **12**, 559–571 (2010).
28. Zurob, H. S. & Seyedrezai, H. A model for the growth of solute clusters based on vacancy trapping. *Scr. Mater.* **61**, 141–144 (2009).
29. Banhart, J., Lay, M. D. H., Chang, C. S. T. & Hill, A. J. Kinetics of natural aging in Al-Mg-Si alloys studied by positron annihilation lifetime spectroscopy. *Phys. Rev. B* **83**, 14101 (2011).
30. Lay, M. D. H., Zurob, H. S., Hutchinson, C. R., Bastow, T. J. & Hill, A. J. Vacancy behavior and solute cluster growth during natural aging of an Al-Mg-Si alloy. *Metall. Mater. Trans. A* **43**, 4507–4513 (2012).
31. Yang, Z. et al. Natural ageing clustering under different quenching conditions in an Al-Mg-Si alloy. *Scr. Mater.* **190**, 179–182 (2021).
32. Pogatscher, S., Antrekowitsch, H., Leitner, H., Ebner, T. & Uggowitzer, P. J. Mechanisms controlling the artificial aging of Al–Mg–Si alloys. *Acta Mater.* **59**, 3352–3363 (2011).
33. Pardoen, T., Dumont, D., Deschamps, A. & Brechet, Y. Grain boundary versus transgranular ductile failure. *J. Mech. Phys. Solids* **51**, 637–665 (2003).
34. Torsæter, M. et al. The influence of composition and natural aging on clustering during preaging in Al–Mg–Si alloys. *J. Appl. Phys.* **108**, 73527 (2010).
35. Dumitraschkewitz, P., Uggowitzer, P. J., Gerstl, S. S. A., Löffler, J. F. & Pogatscher, S. Size-dependent diffusion controls natural aging in aluminium alloys. *Nat. Commun.* **10**, 4746 (2019).
36. Povoden-Karadeniz, E. et al. CALPHAD modeling of metastable phases in the Al–Mg–Si system. *Calphad* **43**, 94–104 (2013).
37. Madanat, M., Liu, M. & Banhart, J. Reversion of natural ageing in Al-Mg-Si alloys. *Acta Mater.* **159**, 163–172 (2018).
38. Pogatscher, S., Antrekowitsch, H., Ebner, T. & Uggowitzer, P. J. in *Light Metals 2012* (ed. Carlos, S.) 415–420 (2012).
39. Gao, G. J. et al. Study of retrogression response in naturally and multi-step aged Al-Mg-Si automotive sheets. *J. Alloys Compd.* **753**, 457–464 (2018).
40. Ding, L. et al. Optimization of the pre-aging treatment for an AA6022 alloy at various temperatures and holding times. *J. Alloys Compd.* **647**, 238–244 (2015).
41. Schmid, F. et al. Effect of thermal treatments on Sn-alloyed Al-Mg-Si alloys. *Materials* **12**, 1801 (2019).
42. Geuser, F. D., Lefebvre, W. & Blavette, D. 3D atom probe study of solute atoms clustering during natural ageing and pre-ageing of an Al-Mg-Si alloy. *Philos. Mag. Lett.* **86**, 227–234 (2006).
43. Pogatscher, S. et al. Influence of interrupted quenching on artificial aging of Al–Mg–Si alloys. *Acta Mater.* **60**, 4496–4505 (2012).
44. Werinos, M. et al. Hardening of Al–Mg–Si alloys. Effect of trace elements and prolonged natural aging. *Mater. Des.* **107**, 257–268 (2016).
45. Zandbergen, M. W., Cerezo, A. & Smith, G. D. W. Study of precipitation in Al–Mg–Si Alloys by atom probe tomography II. Influence of Cu additions. *Acta Mater.* **101**, 149–158 (2015).
46. Peng, J., Bahl, S., Shyam, A., Haynes, J. A. & Shin, D. Solute-vacancy clustering in aluminum. *Acta Materialia* **196**, 747–758 (2020).
47. Zi, Y., Zeqin, L., Leyvraz, D. & Banhart, J. Effect of pre-aging on natural secondary ageing and paint bake hardening in Al-Mg-Si alloys. *Materialia* https://doi.org/10.1016/j.mtla.2019.100413 (2019).
48. Serizawa, A., Hirosawa, S. & Sato, T. Three-dimensional atom probe characterization of nanoclusters responsible for multistep aging behavior of an Al-Mg-Si Alloy. *Metall. Mater. Trans. A* **39**, 243–251 (2008).
49. Morgeneyer, T. F., Starink, M. J., Wang, S. C. & Sinclair, I. Quench sensitivity of toughness in an Al alloy: direct observation and analysis of failure initiation at the precipitate-free zone. *Acta Materialia* **56**, 2872–2884 (2008).
50. Fischer, F. D., Svoboda, J., Appel, F. & Kozeschnik, E. Modeling of excess vacancy annihilation at different types of sinks. *Acta Mater.* **59**, 3463–3472 (2011).
51. Svoboda, J. & Fischer, F. D. Incorporation of vacancy generation/annihilation into reactive diffusion concept—prediction of possible Kirkendall porosity. *Comput. Mater. Sci.* **127**, 136–140 (2017).
52. Poznak, A., Marceau, R. K. W. & Sanders, P. Composition dependent thermal stability and evolution of solute clusters in Al-Mg-Si analyzed using atom probe tomography. *Mat. Sci. Eng. A* **721**, 47–60 (2018).
53. Wenner, S. et al. Clustering and vacancy behavior in high- and low-solute Al-Mg-Si alloys. *Metall. Mater. Trans. A* **45**, 5777–5781 (2014).

54. Gault, B. et al. Advances in the calibration of atom probe tomographic reconstruction. *J. Appl. Phys.* **105**, 34913 (2009).
55. Felfer, P., Ceguerra, A. V., Ringer, S. P. & Cairney, J. M. Detecting and extracting clusters in atom probe data: a simple, automated method using Voronoi cells. *Ultramicroscopy* **150**, 30–36 (2015).
56. Spierings, A. B., Dawson, K., Dumitraschkewitz, P., Pogatscher, S. & Wegener, K. Microstructure characterization of SLM-processed Al-Mg-Sc-Zr alloy in the heat treated and HIPed condition. *Addit. Manuf.* **20**, 173–181 (2018).
57. Miller, M. K & Forbes, R. G. *The Local Electrode Atom Probe* (Springer US, 2014).
58. Dumitraschkewitz, P., Gerstl, S. S. A., Uggowitzer, P. J., Löffler, J. F. & Pogatscher, S. Atom probe tomography study of as-quenched Al-Mg-Si alloys. *Adv. Eng. Mater.* **19**, 1600668 (2017).
59. Svoboda, J., Fischer, F. D. & Fratzl, P. Diffusion and creep in multi-component alloys with non-ideal sources and sinks for vacancies. *Acta Mater.* **54**, 3043–3053 (2006).
60. Pogatscher, S. et al. Process-controlled suppression of natural aging in an Al–Mg–Si alloy. *Scr. Mater.* **89**, 53–56 (2014).
61. Appel, F., Herrmann, D., Fischer, F. D., Svoboda, J. & Kozeschnik, E. Role of vacancies in work hardening and fatigue of TiAl alloys. *Int. J. Plast.* **42**, 83–100 (2013).

Acknowledgements

Financial support from the Christian Doppler Research Association, the Austrian Federal Ministry for Digital and Economic Affairs and the National Foundation for Research, Technology and Development is gratefully acknowledged. The authors also wish to express their sincere thanks to AMAG rolling GmbH for the supply of alloy material. P. D. and S.P. are grateful to the European Research Council (ERC) for the excellent science grant "TRANSDESIGN" through the Horizon 2020 programme under contract 757961. Financial support from the Austrian Research Promotion Agency (FFG) in the project 3DnanoAnalytics (FFG-No. 858040) is also gratefully acknowledged.

Author contributions

F.S., S.P. and P.J.U. conceived the study. F.S. produced the samples and conducted the mechanical testing. T.K. and P.D. performed the measurements. F.S. did the calculations and P.D. and F.S. analysed the data. S.P., P.J.U. and R.T. coordinated and supervised the work. All authors discussed the data extensively. F.S. wrote the paper with the support and correction of all other authors.

Competing interests

The authors declare no competing interests.

Additional information

Supplementary information The online version contains supplementary material available at https://doi.org/10.1038/s43246-021-00164-9.

Correspondence and requests for materials should be addressed to F.S. or S.P.

Peer review information Primary handling editors: Xiaoyan Li, John Plummer.

Reprints and permission information is available at http://www.nature.com/reprints

Publisher's note Springer Nature remains neutral with regard to jurisdictional claims in published maps and institutional affiliations.